A Novel Thermal Energy Storage System in Smart Building Based on Phase Change Material

Wei, Fanrong; Li, Yuanzheng; Sui, Quan; Lin, Xiangning; Chen, Le; Chen, Zhe; Li, Zhengtian

Published in:
IEEE Transactions on Smart Grid

DOI (link to publication from Publisher):
10.1109/TSG.2018.2812160

Publication date:
2019

Document Version
Accepted author manuscript, peer reviewed version

This article has been accepted for publication in a future issue of this journal, but has not been fully edited. Content may change prior to final publication. Citation information: DOI 10.1109/TSG.2018.2812160, IEEE Transactions on Smart Grid

A Novel Thermal Energy Storage System in Smart Building Based on Phase Change Material

Fanrong Wei, Yuanzheng Li, Quan Sui, Xiangning Lin, *Senior Member*, *IEEE*, Le Chen, Zhe Chen, Zhengtian Li

***Abstract*—This paper presents a novel phase change material based thermal energy storage system (PCMTESS) that is suitable for smart building energy management, together with its corresponding thermal-electric combined two-stage dispatching strategy. Benefiting from the phase change materials' thermal characteristic of absorbing or releasing a significant amount of heat at a constant temperature, this thermal energy storage system is endowed with a high capacity and a relatively stable thermal state during its charge/discharge process. To evaluate the thermal performance of the PCMTESS, which is integrated as a part of building wallboard, a detailed analytic thermodynamic building model is proposed that considers the influence of the forced air convection and the external environments, such as solar radiation. Furthermore, a two-stage electric-thermal combined dispatching scheme is designed to minimize the electricity consumption expenditure and power fluctuation on the premise of maintaining a comfortable indoor temperature. Simulation studies on a smart building indicate that the proposed thermal energy storage system is a feasible and economical solution for solving peak load shaving and power fluctuation.**

***Index Terms*—thermal energy storage system, phase change material, analytic building model, electric-thermal combined dispatching**

I. Introduction

THE growing need for clean energy has stimulated a steady increase in the penetration level of renewable energy resources (RES). However, the intermittency and uncertainty from RES bring the problems of peak load shaving and power fluctuation, which raise great challenges to the power balance and reliable operation of the microgrid (MG) [1-2]. Although electric storage systems can be used to address these problems, their disadvantages are evident and include capacity limitations as well as high operation and maintenance costs [3].

Note that thermal loads, such as those generated by an electric water heater (EWH) or air conditioner, contribute to a significant fraction of the overall electricity consumption in residential buildings. Therefore, a thermal energy storage system (TESS) is considered a solution to the problems of peak load shaving and power fluctuation. Ref. [4-5] propose an EWH model to relieve the burden of frequency regulation. Nevertheless, the power consumption of EWH (e.g., 2-3 kWh/day for one family) is much less than air conditioner loads (10-20 kWh/day for a single room). Therefore, this type of energy storage is limited, to some extent, by its capacity. Ref. [6] presents a prototype of a TESS, which stores heat energy in the bricks of a wall to serve as an air conditioner. However, the bricks will reach temperatures of hundreds of degrees Celsius due to their relatively low specific heat capacity, which leads to a rather high insulation requirement for wall envelope structure. Ref. [7-9] show that the thermal energy generated by an air conditioner can be stored in the residential building. In Ref. [10-11], group direct load control and stochastic control models are presented to aggregate loads and regulate end users' behavior. However, restricted by the heat capacity and thermal insulation capability of the residential buildings, the thermal energy stored cannot be retained long enough. Heating, ventilating, and air-conditioning with a water tank can serve as a long-time-scale storage system [12-13]. However, the temperature of the water will fluctuate during the charge/ discharge process, thus impairing the energy storage system's ability to regulate the indoor temperature. In summary, because of the restricted specific heat capacity and unstable thermal state, the effectiveness of the TESS mentioned above still needs to be improved.

To effectively achieve a long–time-scale and large capacity heat transfer, a novel phase change material based thermal energy storage system (PCMTESS) for smart residential building is proposed in this paper. A phase change material (PCM) is a substance that will absorb or release a large amount of heat when it changes from solid state to liquid state with a constant temperature [14]. Taking advantage of the thermal energy storage ability, a number of feasible PCM application schemes have been proposed to reduce the energy consumption of buildings [15-16]. Nevertheless, these schemes are frequently designed to utilize the thermal storage ability in a passive way. However, the PCM can also serve as an active solution to address the load shifting and power balance on the power grid side. In Ref. [17], a model is presented to shape the thermal loads of Google data centers by integrating PCMs into

This work was supported in part by the National Natural Science Foundation of China (No. 51537003 and No. 51707069), in part by Guangxi Power Grid Corporation, in part by the Ministry of Education Key Laboratory of Image Processing and Intelligence Control, Wuhan, China under Grant IPIC2015-01, and the State Key Laboratory of Alternate Electrical Power System with Renewable Energy Sources, North China Electric Power University under Grant LAPS18001.

Fanrong Wei, Quan Sui, Xiangning Lin, Le Chen and Zhengtian Li are with State Key Laboratory of Advanced Electromagnetic Engineering and Technology (Huazhong University of Science and Technology), Wuhan, Hubei 430074 China (e-mail: 453874933@qq.com).

Yuanzheng Li is with the School of Automation, Ministry of Education Key Laboratory of Image Processing and Intelligence Control, Huazhong University of Science and Technology, Wuhan 430074, China, and also with the State Key Laboratory of Alternate Electrical Power System with Renewable Energy Sources, North China Electric Power University, Beijing 102206, China (e-mail: yuanzheng_li@hust.edu.cn).

Z.Chen are with the Department of Energy Technology, Aalborg University, Aalborg, Denmark(E-mail: zch@et.aau.dk)

This article has been accepted for publication in a future issue of this journal, but has not been fully edited. Content may change prior to final publication. Citation information: DOI 10.1109/TSG.2018.2812160, IEEE Transactions on Smart Grid

the data servers. Ref. [18] suggests that PCM based energy storage will be a crucial part of a reliable low-cost grid with 100% renewable energy. However, this specific application of PCM for use with smart buildings has not yet been mentioned. To clarify the above problem, a PCMTESS scheme, together with a detailed analytic thermodynamic model, is proposed in this paper to evaluate the performance of the PCMTESS.

Several works have considered thermodynamic modeling. In [7], an equivalent thermal model is adopted to describe the thermal dynamics of each individual load. A simple model consisting of a differential equation driven by the state of a relay with hysteresis is proposed in [8] to approximate the dominant dynamic of the regulated temperature for air-conditioner systems. A thermodynamic model of the inverter air-conditioner system is presented in [9] to describe the dynamic thermal transition process in a residential building. A simplified equivalent model for the thermal parameters of a residential HVAC unit is proposed in [19] to simulate residential and small commercial buildings. Although the modeling of the thermal systems has been investigated in the literatures above, their models all describe a simplified thermodynamic model that is approximated with sufficient field experiment data that, in turn, reflect only the dominant dynamic process, and the model does not address forced air convection. However, for a thermal storage system that has not yet been built, e.g., the PCMTESS, the field experiment data needed for the model approximation are not available. Further, the thermal output of the PCMTESS includes a forced air convection process, which cannot be approximated by a simplified thermodynamic model. Therefore, a detailed thermodynamic model for PCMTESS is needed.

Subsequently, to solve the multiple time-scale problems simultaneously, a two-stage electric and thermal combined dispatching model is proposed in this paper. Indeed, the two-stage dispatching problem is a research topic of great concern. In Ref. [20-22], a day-ahead scheduling determines economic generation solution based on forecasting data, and the fluctuations caused by forecasting errors are handled with real-time power dispatching. In Ref. [23], a model predictive control is adopted in the two-stage dispatching model to improve the robustness of the control strategy toward forecasting errors. However, for PCMTESS, electric balance is not the only concern: the thermal balance should also be met to keep the indoor temperature comfortable. Meanwhile, the forecasting errors, such as a solar radiation error, will also have an impact on the thermal balance over multiple stages. For electric and thermal combined dispatching, one-stage model predictive control algorithms with an economic objective are adopted in Ref [8, 24], and Ref [9] formulates a model for predictive control strategies to smooth the fluctuations in the solar power generation load with the restriction of thermal comfort. However, only adopting an economic objective will lead to a wide fluctuation of the real-time exchange power, while with a power smoothing objective, the economic value of an energy storage system cannot be validated. Therefore, the proposed dispatching is essential to coordinate the thermal and electric systems to mitigate the impact in multiple time-scales.

TABLE I
THERMOPHYSICAL PROPERTIES OF VARIOUS PCMS

PCM	Melting Point (°C)	Melting Heat (kJ/kg)
n-Hexadecane	16.73	237.72
n-Eicosane	36.63	247.8
Capric acid	30.68	155.5
Lauric acid	42.91	175.8
Myristic acid	52.12	190.0
Palmitic acid	54.13	183.0
Stearic acid	64.52	196.0

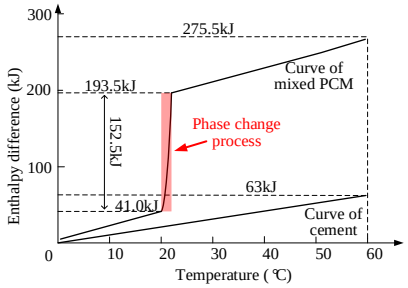

Fig. 1. Enthalpy-temperature relationship of mixed PCM mentioned above

The contributions of this paper are summarized below:

• A novel PCMTESS that is capable of large thermal energy storage in a smart building with a stable thermal state is proposed for the first time. Benefitting from the properties of PCM, the temperature variation of PCMTESS is rather small when its SOC changes from 1 to 0. This is the most significant difference between PCMTESS and other thermal energy storage systems based on sensible heat storage material.

• A detailed mathematic model is presented to analyze the thermal characteristics of the PCMTESS integrated in the wallboard of a smart building. To the best of the authors' knowledge, modelling a thermal storage device which has not yet been built and analyzing its forced air convection process are novel contributions.

• A two-stage electric and thermal combined dispatching method is designed to solve the multiple time-scale electric problems in accounting for the thermal and electric impact of the stochastic solar radiation. With the proposed dispatching method, the energy arbitrage and power smoothing can be achieved at the same time. Meanwhile, the exchange power of the smart building can be updated to the external grid in a day-ahead stage and followed in a real-time stage, thus making the activity of the smart building more predictable.

This paper is organized as follows: Section II introduces a TESS based on PCM. In Section III, an analytic model of the PCMTESS integrated smart building is presented. Section IV introduces a two-stage energy and thermal combined dispatching scheme. Simulation studies are conducted in Section V. Finally, conclusions are drawn in Section VI.

II. STRUCTURE OF A PCM-BASED THERMAL ENERGY STORAGE SYSTEM

In this section, the property of the PCM is briefly introduced, followed by the structural design of a PCM-based thermal energy storage system and its two working modes in a smart building.

A. *Properties of PCM*

As a kind of thermal energy storage medium, PCM has the following advantages:

This article has been accepted for publication in a future issue of this journal, but has not been fully edited. Content may change prior to final publication. Citation information: DOI 10.1109/TSG.2018.2812160, IEEE Transactions on Smart Grid

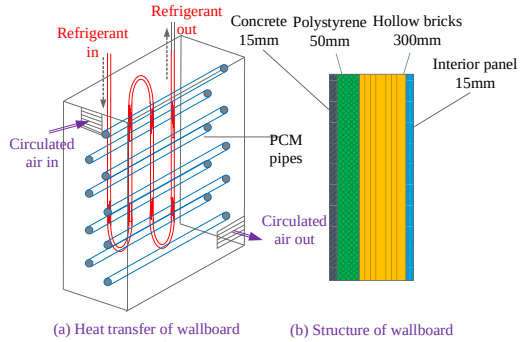

Fig. 2. A typical structure of a PCM-based energy storage wallboard

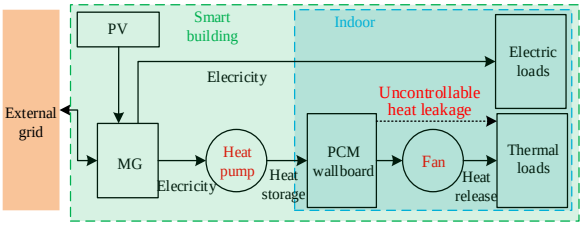

Fig. 3. The structure of the PCMTESS integrated smart building

1) Large heat storage capacity

As shown in Table I, melting heat released or absorbed during the phase change process ranges from 150 to 250 kJ/kg [25]. However, the most commonly used building materials such as cement only absorb 21 kJ/kg when the temperature rises from 40°C to 60°C.

2) Flexible Choice of Melting Point

The melting point can be adjusted by material mixture to satisfy the various demand of thermal storage temperature in different regions. For instance, by mixing capric acid and lauric acid with a weight ratio of 0.6: 0.4, a PCM with a melting point of 20°C and melting heat of 152.5 kJ/kg can be produced, to keep the indoor temperature stable in the 14-20°C range in winter and the 20-26°C range in summer [26].

3) Stable Temperature during the Charge/Discharge Process

As the enthalpy-temperature curve in Fig. 1 shows, the mixed PCM mentioned above can absorb/release a large amount of heat (melting heat) with minor temperature fluctuations.

B. Wallboard Structure of PCMTESS

Based on the PCM introduced above, we propose that a PCMTESS can be established by integrating PCM into the smart building wallboard, in a fashion shown in Fig. 2. The PCMTESS has a function and structure similar to those of a ground heating [27]. The wallboard is composed of a concrete in outer layer, a polystyrene plate in the secondary layer, a hollow brick layer, and the interior panel as the innermost layer. The hollow bricks are densely paved with polyethylene pipes, in which PCMs are encapsulated to prevent PCM leakage and avoid the corrosion of the wallboard [15]. An air gap is arranged between the polyethylene pipes to increase the air contact area, thereby increasing the heat exchange.

The heat pipes are laid in the wallboard within the circulating refrigerant, leading to a direct tight physical contact with the polyethylene pipes. In the process of heat storing, heat pump (HP) converts the electricity into heat, which is transmitted into encapsulated PCM using the refrigerant medium. At present, a similar energy transmission mode is widely adopted in floor heating but with a much larger heat capacity than concrete floor, PCMTESS can achieve better thermal storage performance, with a longer time scale and higher capacity.

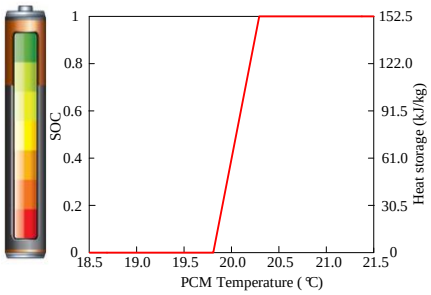

Fig. 4. Definition of PCMTESS SOC and capacity

Only relying on heat conduction and radiation may not meet the needs of indoor temperature control. Therefore, inspired by the circulated air flow in a passive solar-powered green building [28-29], a forced convection with ventilating fan is used to accelerate the heat exchange in a controllable manner, apart from the natural convection and spontaneous heat radiation between the PCM wallboard and the indoor air.

C. Working Modes of PCMTESS

Assume a smart building with a PV panel on the rooftop and PCMTESS in the wallboard, as shown in Fig. 3. The electric loads of the building are directly supplied by the smart building, which can be connected to the external grid, and the indoor temperature regulation service is provided by PCMTESS. The electric-thermal systems are coupled with inverter HPs. There exist two working modes of PCMTESS:

Mode 1: Heat storage mode, where electricity is converted into heat and stored in the PCMTESS with a power balance limitation, and the only controllable device is the HP.

Mode 2: Heat release mode, where heat is released into the room with the thermal balance limitation, and the only controllable device is the ventilating fan.

III. Electric and Thermal Combined Model

As part of the building structure, the precise PCMTESS working status of the heat storage/release should consider the following factors: forced air convection and environmental variables such as the ambient temperature, solar radiation on the wallboards and thermodynamic structure of the building. Therefore, a detailed analytic model combining the electric and thermal energy systems is built to evaluate the working status of the PCMTESS. First, a PV model is presented to serve as the power source of the smart building; then, the energy conversion ratio and SOC of the PCMTESS is defined; finally, a detailed thermodynamic model is proposed to analyze the working status of the PCMTESS on the thermal side.

A. Source Models

The output power of a PV, with respect to the solar radiation power, can be calculated by the following formulation:

$$P_{PV} = G \,/\, 1000 \times P_{PV,rated} \times \eta_{MMPT} \tag{1}$$

This article has been accepted for publication in a future issue of this journal, but has not been fully edited. Content may change prior to final publication. Citation information: DOI 10.1109/TSG.2018.2812160, IEEE Transactions on Smart Grid

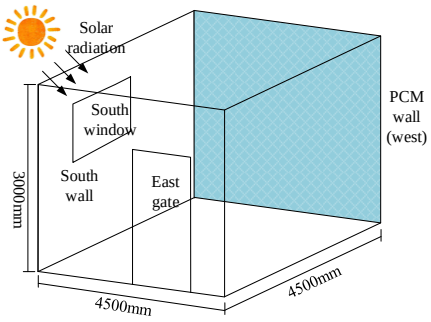

Fig. 5. Simplified block diagram of energy storage building with typical phase change material

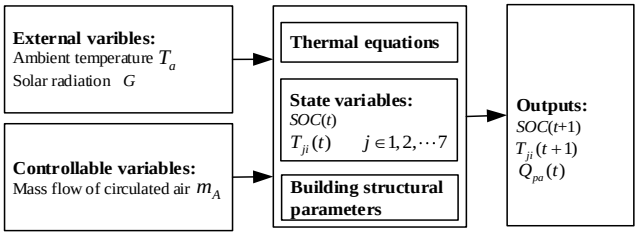

Fig. 6. The input-output relationship of the thermodynamic model

where G is the solar radiation at the array's surface (W/m^2), $P_{PV,rated}$ is the rated power of the PV array at G=1000 W/m^2, and η_{MMPT} is the efficiency of the PV's DC/DC converter in the Maximum Power Point Tracking (MPPT) System. The exchange power between the external grid and the smart building is $P_{GD}(t)$, consisting of the sold power $P_{GD}^{out}(t)$ and the purchased power $P_{GD}^{in}(t)$. $p_{out}\ t$ and $p_{in}\ t$ are the selling price and purchasing price, respectively.

B. PCMTESS Model on Electric Side

The electric heating conversion of HP is formulated as follows:

$$Q_{HP}\ t\ = C_{eh}\ t\ \cdot P_{HP}\ t \tag{2}$$

where $Q_{HP}\ t$ and $P_{HP}\ t$ are the thermal and electric power, respectively, and $C_{eh}\ t$ is the energy efficiency ratio of the inverter HP.

The relationship between SOC/storage capacity and PCM temperature are shown in Fig. 4. The heat capacity $H_p^{\max}$ and SOC can be defined as follows:

$$H_p^{\max} = m_p \cdot \Delta H_p^{\max} \tag{3}$$

$$SOC(t) = H_p(t) \,/\, H_p^{\max} \tag{4}$$

where m_p is mass of the encapsulated PCM and $\Delta H_p^{\max}$ is the enthalpy difference per kilogram between the beginning and end of the phase change process. $H_p(t)$ is the enthalpy of PCMTESS at time t.

C. PCMTESS Model on Thermal Side

Without loss of generality, a PCMTESS-based building is shown in Fig. 5. Assume that the south wall is exposed to solar radiation and that the west wall is integrated with the PCMTESS. The input-output relationship of the PCMTESS building is illustrated as Fig. 6.

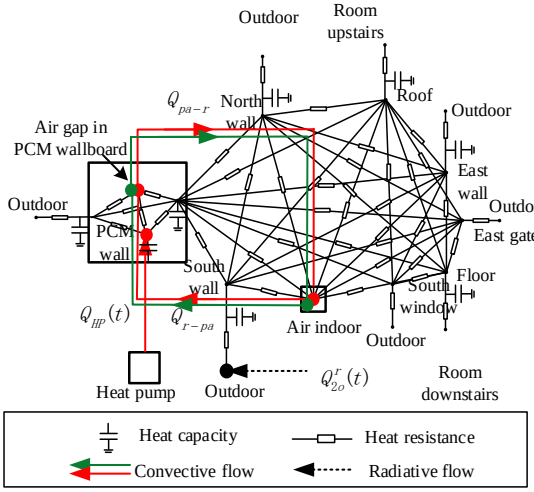

Fig. 7. Thermal network model of PCMTESS in heat storage mode

The variables are defined as follows: T_a is the ambient temperature, and m_A is the flow of circulated air. The state variables are as follows: T_o, T_p, and T_i are the temperature of the outer layer, PCM layer and innermost layer of the PCM wallboard, respectively. T_{ag} is the temperature of air gap in the PCM wallboard, T_r is the indoor temperature of the room space, and T_{1i}, T_{2i}, T_{2o}, T_{3i}, T_{4i}, T_{5i}, T_{6i}, and T_{7i} are the temperatures of south window, inner layer of south wall, outer surface of south wall, east gate, east wall, north wall, the roof and the floor, respectively. In this model, the external variables, G and T_a, are assumed as the known quantities. Assume that the temperatures in the room upstairs and downstairs are the same as this room; therefore, T_{6i} and T_{7i} are equal to T_r.

The typical thermodynamic network model of the PCMTESS in heat storage and heat release mode is shown in Fig. 7, in which the controllable heat exchange is indicated by the red and green lines and the uncontrollable heat exchange is indicated by black lines. Note that the uncontrollable heat exchange process includes two forms: one is heat conduction between the parts in direct contact, and the other is heat radiation between the parts without direct contact, such as the south wallboard to north wallboard. The thermodynamic equations are presented from (5) to (20).

1) Air gap in the PCM wallboard

The air gap in the PCM wallboard is a balanced thermal node. Therefore, the output of the node is the forced air convective flow to the room space, while the input of the node includes the heat flows from PCM pipeline, the outer layer, the innermost layer of wallboard, and the forced air convective flow from the room space. Therefore, the thermodynamic equation of the air gap in a PCM wallboard is given by

$$Q_{ar}(t) = Q_{pa}(t) + Q_{oa}(t) + Q_{ia}(t) + Q_{ra}(t) \tag{5}$$

where $Q_{ar}(t)$ is the forced air convective heat flow from the air gap to the room space and $Q_{pa}(t)$, $Q_{oa}(t)$, $Q_{ia}(t)$, and $Q_{ra}(t)$ are the heat flow from the PCM pipeline, outer layer, innermost layer of wallboard and room space to air gap, respectively.

The expansion of (5) can be expressed by

This article has been accepted for publication in a future issue of this journal, but has not been fully edited. Content may change prior to final publication. Citation information: DOI 10.1109/TSG.2018.2812160, IEEE Transactions on Smart Grid

$$m_A(t)C_A T_{pa}(t) = h_p A_p[T_p(t) - T_a(t)] + h_o A_o[T_o(t) - T_a(t)] + h_i A_i[T_i(t) - T_a(t)] + m_A(t)C_A T_r(t) \quad (6)$$

where C_A is the specific heat capacity of air, A_p, A_o and A_i are air contact areas of the PCM, the outer layer and the innermost layer of wallboard, h_p, h_o and h_i are the convective heat flow coefficients of air with PCM, the outer layer and the innermost layer of wallboard, respectively.

2) Insulated PCM pipeline

In the insulated PCM pipeline, the enthalpy of the PCMTESS can be presented as the function of the temperature $T_p(t)$. Meanwhile, the enthalpy difference equals to the summation of radiation from the outer layer and the innermost layer, the heat flow from heat pump, and subtraction of the convective flow released to the air gap. The thermodynamic equations of the insulated PCM pipeline can be expressed by

$$H_p(t) = \int_{T_{p,0}}^{T_p(t)} m_p C_{pm} dT \quad (7)$$

$$\frac{dH_p(t)}{dt} = -Q_{pa}(t) + Q_{op}^r(t) + Q_{ip}^r(t) + Q_{HP}(t) \quad (8)$$

$$Q_{op}^r(t) = h_{op}^r \left[T_o(t) - T_a(t)\right] \quad (9)$$

$$Q_{ip}^r(t) = h_{ip}^r \left[T_i(t) - T_a(t)\right] \quad (10)$$

where $Q_{op}^r(t), Q_{ip}^r(t)$ is the radiative heat flow from the outer/ innermost layer to PCM pipeline, C_{pm} is the specific heat capacity during the phase change process, $T_{p,0}$ is the starting temperature point of the phase change process, and h_{op}^r, h_{ip}^r are the radiative heat flow coefficients of PCM pipeline with the outer layer and the innermost layer of wallboard, respectively.

Combining equations (7) and (8), we have

$$m_p C_{pm} \frac{dT_p(t)}{dt} = -Q_{pa}(t) + Q_{op}^r(t) + Q_{ip}^r(t) + Q_{HP}(t) \quad (11)$$

Equation (11) can be transformed into its discrete form over discrete intervals of 1 as

$$m_p C_{pm} \left[T_p(t+1) - T_p(t)\right] = -Q_{pa}(t) + Q_{op}^r(t) + Q_{ip}^r(t) + Q_{HP}(t) \quad (12)$$

Combining (12) with (9) -(10), we have

$$m_p C_{pm} \left[T_p(t+1) - T_p(t)\right] = -h_p A_p[T_p(t) - T_a(t)] + h_{op}^r \left[T_o(t) - T_a(t)\right] + h_{ip}^r \left[T_i(t) - T_a(t)\right] + Q_{HP}(t) \quad (13)$$

The same discrete form can be applied to 11-13 and 14-16 as well. In this way, problem (21) is converted into an MILP.

3) Inner and outer layers of PCM wallboard

The thermodynamic equations of the inner and outer layers of the PCM wallboard can be expressed by

$$Q_{am}(t) = Q_{out}^c(t) \quad (14)$$

$$Q_{out}^c(t) = m_o \frac{dH_o}{dt} - Q_{oa}(t) - Q_{op}^r(t) \quad (15)$$

$$-Q_{ia}(t) - Q_{ip}^r(t) = m_i \frac{dH_i}{dt} + Q_{ir}(t) + \sum_{i=1}^{n} Q_{pwi\text{-}i}^r(t) \quad (16)$$

where $Q_{am}(t)$ is the convective heat flow between the exterior surface of outer layer and outside ambient and m_o, m_i and H_o, H_i are the mass and enthalpy per kilogram of the inner and outer layers of PCM wallboard, respectively. $Q_{out}^c(t)$ is the conductive heat flow between the exterior and inner surface of outer layer, and $Q_{ir}(t)$ and $Q_{pwi-i}^r(t)$ are the heat flow from the inner layer of PCM wallboard to the indoor air and other walls, respectively.

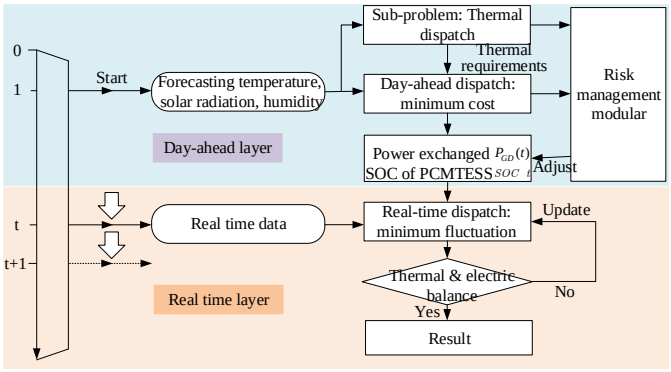

Fig. 8. Flowchart of two-stage electric and thermal combined dispatching

4) Other wallboards

Taking the south wall, which is exposed to solar radiation, as an example, we have

$$Q_{2o}^r(t) = \alpha_{sw} G \quad t \quad (17)$$

$$Q_{2o}^r(t) + Q_{Am-2o}(t) = Q_{2o-2i}^c(t) \quad (18)$$

$$Q_{2o-2i}^c(t) = m_2 \frac{dH_2}{dt} + Q_{2i-r}(t) + \sum_{j=1, j\neq 2}^{n} Q_{2i-ji}(t) \quad (19)$$

where $Q_{2o}^r(t)$ is the solar radiation to the exterior surface of south wall, α_{sw} is the radiation absorption coefficient of the wall, $Q_{am-2o}(t)$ is the convective heat flow between the exterior surface of the south wall and the outside ambient conditions, $Q_{2o-2i}^c(t)$ is the conductive heat flow between the exterior and inner surface of south wall, m_2 and H_2 are mass and enthalpy per kilogram of south wall, and $Q_{2i-r}(t)$ and $Q_{2i-ji}(t)$ are the heat flow from south wall to indoor air and other walls, respectively.

5) Indoor air

$$Q_{ir}(t) = Q_{ra}(t) + \sum_{i=1}^{n} Q_{ri}(t) \quad (20)$$

where $Q_{ri}(t)$ is the convective heat flow between the indoor air and the building envelope.

The thermodynamic equations from (5) to (20) can be solved simultaneously to obtain the variables of the indoor temperature, heat exchange and SOC of PCMTESS, based on the two-stage electric and thermal combined dispatching model that is presented in Section IV.

IV. Two-stage Electric and Thermal Combined Dispatching Model

As shown in Fig. 8, a two-stage dispatching model is proposed for a smart building. This model is composed of the day-ahead stage and the real-time stage. The day-ahead dispatching in the upper stage first solves the sub-problem of thermal dispatching to supply the day-ahead predictive heat

This article has been accepted for publication in a future issue of this journal, but has not been fully edited. Content may change prior to final publication. Citation information: DOI 10.1109/TSG.2018.2812160, IEEE Transactions on Smart Grid

requirements and then optimizes the exchange power between the smart building and the external grid with the objective of minimum cost. Subsequently, the derived exchange power from the day-ahead stage is used to guide the real-time dispatching. The forecast error may lead to a risk of SOC violation by the PCMTESS. To solve this, a risk management module is conducted to appropriately adjust the exchange power. During real-time operation, actual solar and ambient temperature data are available. In this case, the negative impacts due to a forecasting error of the electric and thermal system can be mitigated by real-time MPC dispatching.

A. Day-ahead Dispatching Stage

1) Thermal sub-problem

With the controllable flow of circulated air and uncontrollable heat leakage, the heat consumption should be optimized with thermal constraints, which can be presented as follows:

$$T_{\min}(t) \le T_r(t) \le T_{\max}(t) \tag{21}$$

$$0 \le m_A \le m_{A\text{-max}} \tag{22}$$

where $m_{A\text{-max}}$ is the maximum mass of forced air convection and $T_{\min}(t)$ and $T_{\max}(t)$ are the upper and lower limits of the comfortable temperature, respectively. As proposed in many papers and in the ISO 7730 standard [30], thermal comfort is mainly decided by four environment factors (air temperature, air relative humidity, air velocity, and mean radiant temperature) and two individual factors (activity level and clothing insulation). When these factors are estimated or measured, the thermal sensation can be predicted by calculating the PMV and PPD. Thus, with an expected PMW/PPD target, we can calculate an expected $T_{\min}(t)$ and $T_{\max}(t)$.

However, accurately estimating all these parameters a day in advance is not always possible. To reduce the input parameters of the ISO 7730 model, Ref. [31] proposes a simplified thermal comfort model with only the air temperature and relative humidity, which can provide a good approximation for the ISO 7730 model. Thus, the simplified thermal comfort model is presented as follows, and the detailed model is found in [31].

$$PPD = 100 - 95 \cdot \exp(-0.03353 \cdot PMV^4 - 0.2179 \cdot PMV^2) \tag{23}$$

$$PMV = a \cdot T_a + b \cdot P_v - c \tag{24}$$

$$P_v = rh \cdot 10 \cdot e^{(16.6536 - 4030.183)/(T_r + 273)} \tag{25}$$

where a, b, and c are the coefficients in [31], P_v is vapor pressure in ambient air, and rh is the relative air humidity.

The thermal sub-problem is optimized to evaluate the minimum 24-hour thermal output of the PCMTESS $Q_{pa}(t)$, which will be supplied by multiple heat transfer methods, i.e., the heat leakage (uncontrollable) and the forced air convection (controllable). During the heat transfer process, $m_A(t)$ serves as the only controllable element of the thermal storage system and is restricted with explicit upper and lower boundaries. The thermal output is determined by the controllable forced air convection, and the controllable forced air convection is decided by $m_A(t)$. Therefore, $m_A(t)$ is an intermediate variable for predicting $Q_{pa}(t)$. Therefore, the objective of sub-problem F_{sp} is to minimize the summation of controllable heat exchange, which can be represented by $m_A(t)$. F_{sp} is formulated as follows:

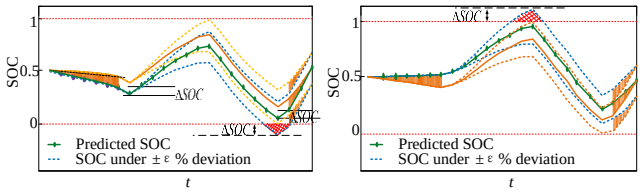

(a) Upper limit of SOC (b) Lower limit of SOC

Fig. 9. Flowchart of two-stage electric and thermal combined dispatching

$$F_{sp}: \min \sum_{t=1}^{N} m_A(t) \qquad \forall t \tag{26}$$

$$\text{s.t.} \quad (5)\text{-}(22)$$

By optimizing (26), the minimum thermal output of PCMTESS $Q_{pa}(t)$ can be acquired, and the thermal input of PCMTESS is the heat supplied by heat pumps via the consumption of electricity. Therefore, the thermal and electric problems can be linked through the SOC of the PCMTESS, which can be expressed by (27) and (28), respectively.

$$H_p(t+1) = H_p(t) + Q_{HP}(t) - Q_{pa}(t) \tag{27}$$

$$SOC(t+1) = H_p(t+1) / H_p^{\max} \tag{28}$$

2) Electric and thermal combined dispatching

The objective function of electric side F_d minimizes the expected electricity cost of the smart building, which is formulated as follows:

$$F_d: min \sum_{t=1}^{N} P_{GD}^{in}(t) \cdot p_{in}(t) - P_{GD}^{out}(t) \cdot p_{out}(t) \tag{29}$$

$$\text{s.t.} \quad \sum_{i=1}^{N_{PV}} P_{PV,i}(t) + P_{GD}(t) = \sum_{i=1}^{N_{HP}} P_{HP,i}(t) + \sum_{i=1}^{N_E} P_{E-load,i}(t) \qquad \forall t \tag{30}$$

$$0 \le P_{HP}(t) \le P_{HP}^{max} \qquad \forall t \tag{31}$$

$$H_p(t_0) = H_p(t_N) \tag{32}$$

$$0 \le SOC(t) \le 1 \qquad \forall t \tag{33}$$

In addition, the exchange power of the smart building is expected to be equal to each other to serve as a constant load among the off-peak hours:

$$P_{GD}(i) = P_{GD}(j) \quad i, j \in off\text{-}peak \cdot hours \tag{34}$$

Restricted by the SOC of PCMTESS and the power balance, the exchange power of the smart building with the external grid $P_{GD}(t)$ is optimized to minimize the electricity cost. It can be seen that the exchange power $P_{GD}(t)$ and SOC of PCMTESS $SOC(t+1)$ are the elements set in the day-ahead stage, and applied to guide the real-time dispatching. Meanwhile, $P_{GD}(t)$ is updated to the external grid to serve as a predictable load.

3) Risk Management Module

To guarantee the scheduling solutions to accommodate extreme solar radiation fluctuation, the SOC of PCMTESS should satisfy the restriction under the extreme scenarios that the solar radiation deviate by ε% (or − ε%) from the forecast values. Define ΔSOC as the maximum deviation of SOC from

This article has been accepted for publication in a future issue of this journal, but has not been fully edited. Content may change prior to final publication. Citation information: DOI 10.1109/TSG.2018.2812160, IEEE Transactions on Smart Grid

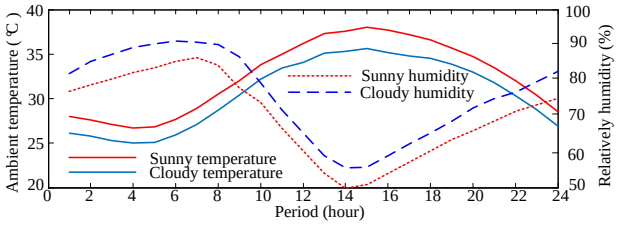

Fig. 10. Typical curves of ambient temperature and humidity

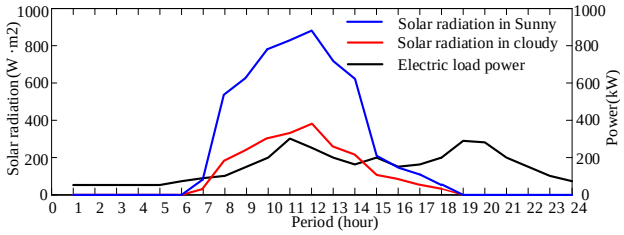

Fig. 11. Curves of outdoor solar radiation intensity and electric load

the upper or lower boundaries, as shown in Fig. 9. The adjustment of exchange power should be conducted between the off-peak hours as follows:

$$\begin{cases} \sum_{t=0}^{m} \Delta P_{GD}^{in}(t) = \Delta SOC \cdot H_{PCMTESS}^{\max} & m \in offpeak\text{-}morning \\ \sum_{t=22}^{n} \Delta P_{GD}^{in}(t) = -\Delta SOC \cdot H_{PCMTESS}^{\max} & n \in offpeak\text{-}night \end{cases} \quad (35)$$

B. Real-time Dispatching Stage

As a predictable load, the smart building will update the optimized exchange power to the external grid in the day-ahead stage. However, the prediction errors of solar radiation and ambient temperature will result in a fluctuation of the exchange power. Meanwhile, the indoor temperature will be influenced by these prediction errors. Therefore, a MPC on the thermal and electric sides is implemented to compensate for prediction errors.

The thermal sub-problem in the real-time stage F_{rsp} is to minimize the controllable heat exchange in the prediction horizon while tracking the prediction errors. M is the prediction horizon of the MPC.

$$F_{rsp}: \min \sum_{\tau=t}^{t+M-1} m_A(\tau) \quad \forall\tau \quad (36)$$

s.t. (5)- (22)

The objective function of electric side of the system in the real-time stage F_{rd} minimizes the deviation of exchange power between the value updated in the day-ahead stage and the external grid, and the SOC at the end of the prediction horizon should match the day-ahead one. Therefore, F_{rd} is formulated as follows:

$$F_{rd}: min \sum_{\tau=t}^{t+M-1} \left(\left| \hat{P}_{GD}^{in}(\tau) - P_{GD}^{in}(\tau) \right| + \left| \hat{P}_{GD}^{out}(\tau) - P_{GD}^{out}(\tau) \right| \right) \quad (37)$$

s.t. $\overset{\wedge}{SOC}(t+M-1) = SOC(t+M-1)$

(30) -(33)

where the $\wedge$ operator is used to denote an estimated state or quantity at times when the value is unknown.

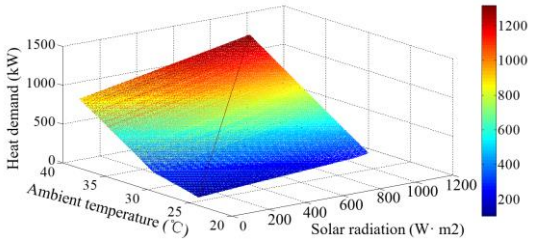

Fig. 12. Correlation among thermal demand, ambient temperature and solar radiation

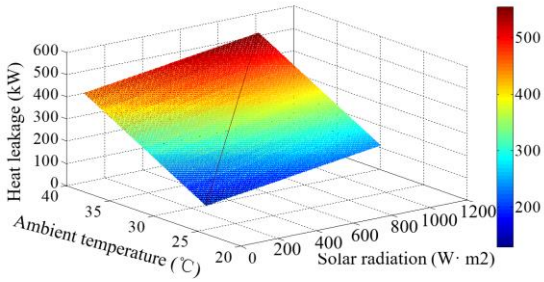

Fig. 13. Heat leakage of PCMTESS without forced air convection

V. Numerical Simulations

In this section, the basic property of the PCMTESS is analyzed, the performance of the PCMTESS in the day-ahead and real-time stages is presented and the two-stage thermal and electric combined dispatching is compared with a typical one-stage dispatching to prove its advantage. Finally, a cost analysis is conducted to validate the economic value of the proposed PCMTESS.

A. Test System

A grid-connected smart building, shown in Fig. 3, is established to verify the effectiveness of the PCMTESS, which contains a 1500 kW rooftop PV and 400 rooms in total, each with a 3 kW HP and 1000 kg PCM integrated wallboard. The efficiency of HP is set to 2.6. In China, the off-peak hours are 0:00-6:00 and 22:00-24:00, and the on-peak hours are 6:00-22:00. The electricity price is set as 0.3 Yuan/kWh during off-peak, 0.7 Yuan/kWh during on-peak and 0.2 Yuan/kWh when sold to the external grid. The length, width and height of all the rooms are set as 4500 x 4500 x 3000 mm, the thermodynamic parameters are set according to Ref. [32-34], and $m_{A\text{-}\max}$ is set as 5 kg/s. The contact surface of the PCM is 500% of the wallboard. The typical curves of ambient temperature, humidity and solar radiation in the summer are shown in Figures 10 and 11 [35].

All numerical simulations are coded in MATLAB and solved using Yalmip. The running time of each case is 1-5 minutes on a 4.0 GHz Windows-based PC with 8 GB of RAM.

B. Analysis of Basic PCMTESS Properties

1) Thermal demand of PCMTESS building

To analyze the thermal demand of a PCMTESS building, the correlation among the thermal demand, ambient temperature and solar radiation is shown in Fig. 12. With a constant humidity (set as 70% in Fig. 12), the heat demand of the building with an indoor temperature of 26 ℃ is determined by

This article has been accepted for publication in a future issue of this journal, but has not been fully edited. Content may change prior to final publication. Citation information: DOI 10.1109/TSG.2018.2812160, IEEE Transactions on Smart Grid

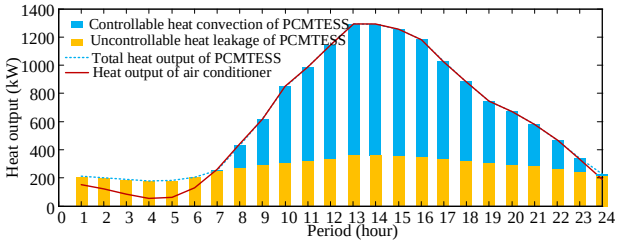

Fig. 14. Multiple heat transfer in sunny days

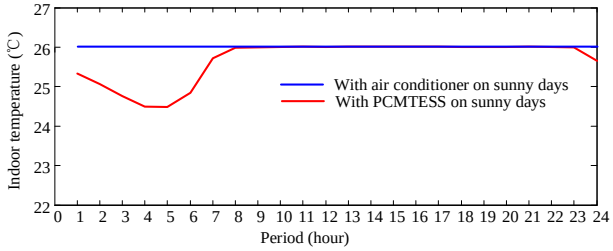

Fig. 15. Indoor air temperature on sunny days

both the solar radiation and ambient temperature. For instance, the heat demand rises nearly 40% at an ambient temperature of 37 ℃, and the solar radiation changes from 0 W/m^2 to 1000 W/m^2. Consequently, ignoring the influence of solar radiation will lead to significant estimation error, which verifies the importance of the thermodynamic analysis model.

2) Heat Leakage of PCMTESS without Forced Air Convection

Comparing Figures 12 and 13, it can be seen that the uncontrollable heat leakage can release some heat into the building, but it is insufficient to keep an indoor temperature of 26 ℃, which means that it is also insufficient to keep the indoor air temperature at 26 ℃ without the use of forced air convection. As a consequence, it is essential to use multiple methods of heat transfer to keep the indoor temperature comfortable at all times.

3) Multiple Heat Transfer Methods and Indoor Air Temperature

With the meteorological data of sunny days shown in Fig. 10, the multiple heat outputs of the PCMTESS are presented in Fig. 14. It can be seen that the heat demand in the 0:00-7:00 time period is satisfied only by heat leakage and is supported by forced air convection during other periods. Compared with fully controllable equipment, such as an air conditioner, the multiple methods of heat transfer outputs more during the 0:00-7:00 time period.

As shown in Fig. 15, the indoor temperature using the air conditioner is always kept at 26 ℃, which is the same temperature that the PCMTESS maintains for most hours. However, the temperature of the PCMTESS-cooled system will be 1 ℃-2 ℃ lower than the upper limit during 0:00-7:00. The reason is that the air conditioner is fully controllable, whereas PCMTESS has controlled forced heat convection but uncontrollable with heat leakage.

C. Performance of PCMTESS in Day-ahead and Real-time Stage

1) Electric Consumption of PCMTESS and Air Conditioner in Day-ahead Stage

As shown in Fig. 16 (a), for a smart building with an air conditioner operating in a sunny day, the power requirement of the air conditioner cannot follow the variation of PV output (during 7:00- 15:00) since the PV output is abundant during this

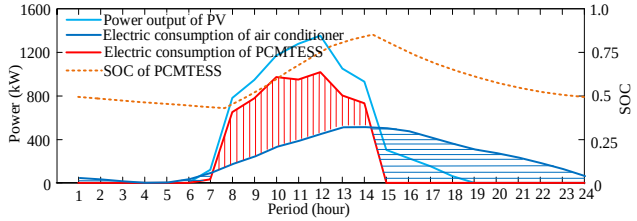

(a) Electricity consumption on a sunny day

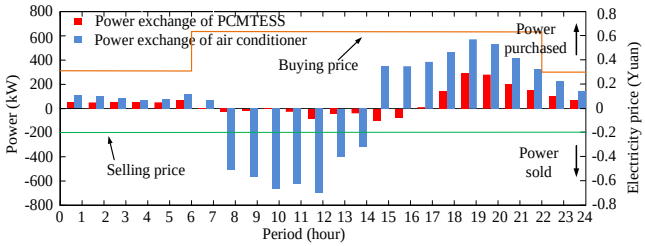

(b) Exchange power on a sunny day

Fig. 16. Electricity consumption and power exchange in a sunny day

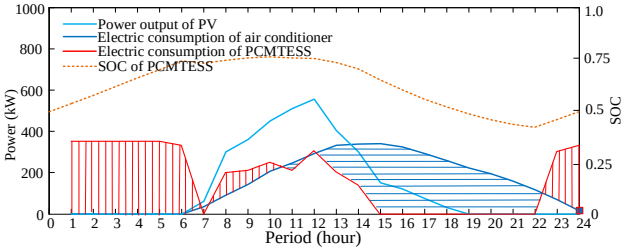

(a) Electricity consumption on a cloudy day

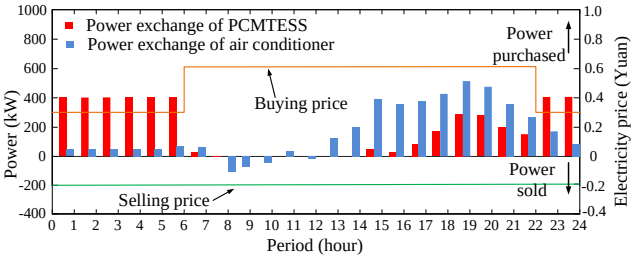

(b) The exchange power in a cloudy day

Fig. 17. Electricity consumption and power exchange in a cloudy day

period of time and exceeds the necessary power input of the air conditioner to maintain a comfortable room temperature. In this case, the excessive power must be fed back to the external grid with a relatively low selling price (0.2 Yuan/kWh), as shown in Fig. 16 (b). This is because that the power of the air conditioner is rigidly associated with the external environment when keeping the room temperature. However, during 15:00-22:00, a building with an air conditioner must buy a large quantity of electricity from the external grid at the peak price (0.7 Yuan/kWh) to satisfy its thermal demand because the PV output is insufficient. In comparison, in a smart building with PCMTESS, its power requirements are basically capable of following the variation of PV output while the PV output is abundant. From 15:00-22:00, there is no power consumption by the PCMTESS. Instead, the thermal demand of the building is satisfied by the heat stored in the PCM in advance, accomplishing the objective to shift the thermal load from peak hours to the PV abundant hours.

As calculated by (29), the expenditures of a building with an air conditioner and PCMTESS are 2455 Yuan and 981 Yuan, respectively, which means that PCMTESS can save 1474 Yuan

This article has been accepted for publication in a future issue of this journal, but has not been fully edited. Content may change prior to final publication. Citation information: DOI 10.1109/TSG.2018.2812160, IEEE Transactions on Smart Grid

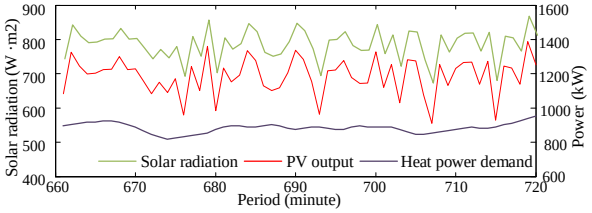

(a) Real-time correlation between PV output and heat demand

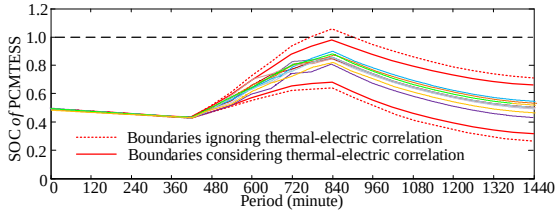

(b) SOC of PCMTESS under 20% stochastic prediction error

Fig. 18. Robustness analysis of day-ahead dispatching

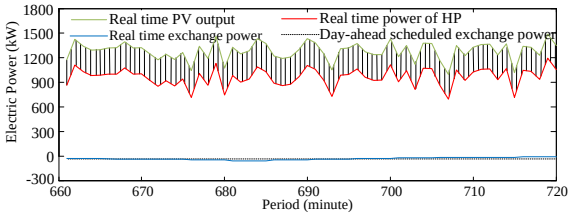

(a) Electric balance recovery by HP power tracking

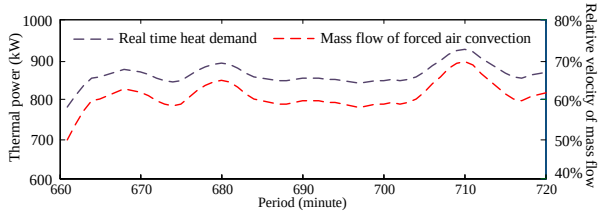

(b) Thermal balance recovery by mass flow adjusting of circulated air

Fig. 19. Typical curves of outdoor solar radiation intensity

for the building residents on a sunny day. In addition, the maximum power during the peak hours of the two schemes are 586 kW and 272 kW, respectively, indicating that a smart building with PCMTESS has a significantly lower and smoother power exchange and is friendlier to the external grid. For the scenario involving a cloudy day with insufficient PV output in Fig. 17, compared with the building with air conditioner, the thermal demand of PCMTESS at the peak hours is shifted to valley hours. The expenditures of the building with air conditioner and PCMTESS are 2731 Yuan and 1864 Yuan, respectively, which means that PCMTESS can save 867 Yuan for the building residents on a cloudy day. The maximum power of the two schemes are 619 kW and 400 kW, respectively, indicating that the smart building with PCMTESS is still friendlier to the external grid.

2) Robustness Analysis

Fig. 18 shows the robustness analysis of day-ahead dispatching. The correlation between PV output and heat demand during 11:00-12:00 on sunny days is presented in Fig. 18(a). It can be seen that the real-time heat demand and PV output will rise and fall simultaneously and that the heat demand curve will become smoother due to the heat capacity of the building parts. As shown in Fig. 18(b), the SOC of PCMTESS under a 20% stochastic prediction error does not exceed the upper and lower boundaries estimated in the day-ahead prediction, and the boundaries while considering the thermal-electric correlation are more precise.

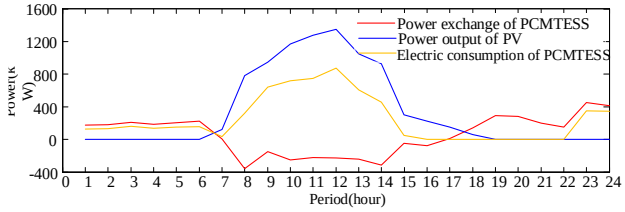

(a) Electricity consumption with one-stage dispatching on a sunny day

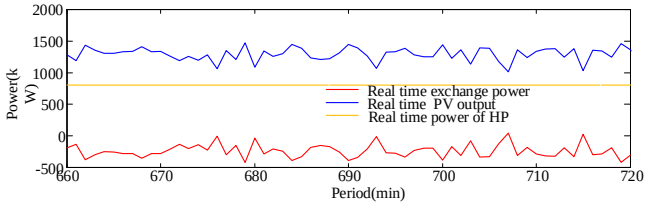

(b) Real-time electric balance with one-stage dispatching on a sunny day

Fig. 20. Typical day-ahead and real-time curves with one-stage dispatching

TABLE II

OPERATION COST OF THE SMART BUILDING IN SUMMER

Weather	Thermal element	Electricity purchased (kWh)		Electricity sold (kWh)	Cost (Yuan)
		On-peak	Off-peak		
Sunny	PCMTESS	1,260	612	423	981
	Air conditioner	4,088	1,163	3,778	2,455
	Green building	4,088	1,163	3,778	2,455
Cloudy	PCMTESS	1,285	3,215	0	1,864
	Air conditioner	3,722	574	232	2,731
	Green building	3,421	550	569	2,446

3) Electric and Thermal Balance in Real-time Stage

Fig. 19 shows the real-time electric and thermal balance recovery under the solar radiation fluctuation presented in Fig. 18 (a). The electric-thermal balance is achieved through HP power tracking and adjusting the flow of circulated air, respectively. Compared with the directly controlled air conditioner that only controls the electric side and makes the temperature indoor fluctuate within its limitations, the decoupling of thermal and electric control makes it possible to satisfy the temperature comfort and stable exchange power goals simultaneously. While the dispatching model in the real-time stage is improved with MPC, the blue line in Fig. 19 (a) indicates that the real-time exchange power will be almost the same as that scheduled in the day-ahead stage.

D. Comparison with One-stage Dispatching

A one-stage MPC dispatching model with the objective of minimizing the electricity cost in [9] is presented for comparison with the proposed two-layer dispatching model. The exchange power curves scheduled in the day-ahead and real-time stages are presented as Fig. 20 (a) and Fig. 20 (b). Comparing Fig. 20 (a) and Fig. 20 (b) with Fig. 17 (a) and Fig. 19 (a), the improvements of two-stage dispatching model related to the one-stage model can be presented as follows:

1) On the economic level, the electricity cost of the proposed dispatching model is 1,407 Yuan, which is smaller than 1,754 Yuan, the electricity cost of the one-stage model.

2) The exchange power smoothing and prediction error correction can be implemented in the real-time stage with the proposed two-stage model, but it cannot be realized with this one-stage model.

E. Economic Analysis

Three typical thermal loads or thermal relative energy storage units, i.e. air conditioning, a green building with PCM proposed in [28] and PCMTESS are compared in terms of operation costs, as shown in Tab. II. The parameters of the passive green building with PCM are from [28]. Calculate the economic benefits in accordance with the following scenarios: 120 days of air conditioning service period every summer, including 60% sunny days and 40% cloudy days. Compared to the other two schemes, t the application of PCMTESS can cut down expenses for 147,744 Yuan and 134,064 Yuan each summer. Assume that the heating season is 90 days, including 40% of sunny days and 60% of cloudy days. The typical whether data are from Wuhan, CN [36], the savings of PCMTESS scheme are calculated as 79,854 Yuan and 79,854 Yuan. In summary, if adopting the scheme of PCMTESS, the annual savings will be 227,598 Yuan and 213,918 Yuan.

There are 400 sets of PCMTESS, and the cost for each one includes 1000kg of PCM for 3,000 Yuan and auxiliary systems costs for 3,500 Yuan. Compared to the cost of an air conditioner for 2,500 Yuan, and green building with PCM for 3,500 Yuan, the extra investments of PCMTESS are 1,600,000 Yuan and 1,200,000 Yuan for this smart building. Thus the payback periods of the extra investments are 7.03 years and 5.61 years, far lower than the service life of PCMTESS, which is nearly 30 years [15].

VI. CONCLUSION

In this paper, we have proposed a novel thermal energy storage system with a high energy capacity and stable thermal status. To evaluate the thermal and economic performance of PCMTESS, a comprehensive electric-thermal combined analytical model and a two-stage dispatching scheme are proposed. The simulation study shows that PCMTESS can keep the room temperature in a comfort range, and the design of integrating PCM into the wall utilizes the heat leakage well.

With the two-stage dispatching scheme, PCMTESS stores the excess power of a smart building on sunny days while achieving peak load shaving and valley filling on cloudy days. Therefore, the operation cost of a smart building is largely reduced, and the power and indoor temperature fluctuation can be mitigated by real-time thermal-electric control.

REFERENCES

[1] P. Samadi, V. W. S. Wong and R. Schober, "Load scheduling and power trading in systems with high penetration of renewable energy resources," *IEEE Trans. Smart Grid*, vol. 7, no. 4, pp. 1802-1812, July 2016.

[2] W. Su, J. Wang and J. Roh, "Stochastic energy scheduling in microgrids with intermittent renewable energy resources," *IEEE Trans. Smart Grid*, vol. 5, no. 4, pp. 1876-1883, July 2014.

[3] V. Boicea, "Energy storage technologies: The past and the present," *Proc. IEEE*, vol. 102, no. 11, pp. 1777–1794, Nov. 2014.

[4] M. Shad, A. Momeni, R. Errouissi, C. P. Diduch, M. E. Kaye and L. Chang, "Identification and estimation for electric water heaters in direct load control programs," *IEEE Trans. Smart Grid*, vol. 8, no. 2, pp. 947-955, March 2017.

[5] Z. Xu, R. Diao, S. Lu, J. Lian and Y. Zhang, "Modeling of electric water heaters for demand response: a baseline PDE model," *IEEE Trans. Smart Grid*, vol. 5, no. 5, pp. 2203-2210, Sept. 2014.

[6] S. Wong and J. P. Pinard, "Opportunities for smart electric thermal storage on electric grids with renewable energy," *IEEE Trans. Smart Grid*, vol. 8, no. 2, pp. 1014-1022, March 2017.

[7] W. Zhang, J. Lian, C. Y. Chang and K. Kalsi, "Aggregated modeling and control of air conditioning loads for demand response," *IEEE Trans. Power Syst.*, vol. 28, no. 4, pp. 4655-4664, Nov. 2013.

[8] N. Mahdavi, J. H. Braslavsky, M. M. Seron and S. R. West, "Model predictive control of distributed air-conditioning loads to compensate fluctuations in solar power," *IEEE Trans. Smart Grid*, vol. PP, no. 99, pp. 1-1.

[9] M. Song, C. Gao, H. Yan and J. Yang, "Thermal battery modeling of inverter air conditioning for demand response," *IEEE Trans. Smart Grid*, vol. PP, no. 99, pp. 1-1.

[10] H. T. Nguyen, D. T. Nguyen and L. B. Le, "Energy management for households with solar assisted thermal load considering renewable energy and price uncertainty," *IEEE Trans. Smart Grid*, vol. 6, no. 1, pp. 301-314, Jan. 2015.

[11] N. Forouzandehmehr, M. Esmalifalak, H. Mohsenian-Rad and Z. Han, "Autonomous demand response using stochastic differential games," *IEEE Trans. Smart Grid*, vol. 6, no. 1, pp. 291-300, Jan. 2015.

[12] D. H. Blum, T. Zakula and L. K. Norford, "Opportunity cost quantification for ancillary services provided by heating, ventilating, and air-conditioning systems," *IEEE Trans. Smart Grid*, vol. 8, no. 3, pp. 1264-1273, May 2017.

[13] Y. J. Kim, D. H. Blum, N. Xu, L. Su and L. K. Norford, "Technologies and magnitude of ancillary services provided by commercial buildings," *Proc. of the IEEE*, vol. 104, no. 4, pp. 758-779, April 2016.

[14] Zhou, D., C. Y. Zhao, and Y. Tian. "Review on thermal energy storage with phase change materials (PCMs) in building applications," *Appl. Energy*, vol. 92, no. 4, pp. 593-605, Feb. 2012.

[15] Tyagi, V. V., et al. "Development of phase change materials based microencapsulated technology for buildings: A review," *Renew. & Sustain. Energy Reviews*, vol. 15, no. 2, pp. 1373-1391, May 2011.

[16] Gracia A D, Cabeza L F. "Phase change materials and thermal energy storage for buildings," *Energy & Buildings*, vol. 103, pp. 414-419, Sep. 2015.

[17] Skach, Matt, et al. "Thermal time shifting: decreasing data center cooling costs with phase-change materials," *IEEE Internet Computing*, vol. 9, no. 9, pp. 1-1, 2017.

[18] Jacobson, Mark Z., et al. "100% Clean and renewable wind, water, and sunlight (WWS) all-sector energy roadmaps for the 50 United States," *Energy & Environmental Science*, vol. 8, no. 7, pp. 2093-2117, 2015.

[19] N. Lu, "An evaluation of the HVAC load potential for providing load balancing service," *IEEE Trans. Smart Grid*, vol. 3, no. 3, pp. 1263-1270, Sep. 2012.

[20] Q. Jiang, M. Xue, and G. Geng, "Energy management of microgrid in grid-connected and stand-alone modes," *IEEE Trans. Power Syst.*, vol. 28, no. 3, pp. 3380–3389, Aug. 2013.

[21] T. Logenthiran, D. Srinivasan, A. M. Khambadkone, and H. N. Aung, "Multi-agent system for real-time operation of a microgrid in real-time digital simulator," *IEEE Trans. Smart Grid*, vol. 3, no. 2, pp. 925–933, Jun. 2012.

[22] Z. Zhang, J. Wang, T. Ding and X. Wang, "A two-layer model for microgrid real-time dispatching based on energy storage system charging /discharging hidden costs," *IEEE Trans. Sustain. Energy*, vol. 8, no. 1, pp. 33-42, Jan. 2017.

[23] S. Raimondi Cominesi, M. Farina, L. Giulioni, B. Picasso and R. Scattolini, "A two-layer stochastic model predictive control scheme for microgrids," *IEEE Trans. Control Syst. Tech.*, vol. PP, no. 99, pp. 1-13.

[24] M. Brandstetter, A. Schirrer, M. Miletić, S. Henein, M. Kozek and F. Kupzog, "Hierarchical Predictive Load Control in Smart Grids," *IEEE Trans. Smart Grid*, vol. 8, no. 1, pp. 190-199, Jan. 2017.

[25] Liu, Cheng, et al. "A novel PCM of lauric–myristic–stearic acid/expanded graphite composite for thermal energy storage," *Materials Letters*, vol. 120, no. 4, pp. 43-46, April 2014.

[26] Wang Y, Xia T D, Zheng H, et al. "Stearie acid/silica fume composite as form-stable phase change material for thermal energy storage," *Energy & Buildings*, vol. 43, pp. 2365-2370, Sep. 2011.

[27] Bi Y, Wang X, Liu Y, et al. "Comprehensive energy analysis of a ground-source heat pump system for both building heating and cooling modes," *Applied Energy*, vol. 86, no. 12, pp. 2560-2565, Dec. 2009.

[28] G.Hed, R.Bellander. "Mathematical modelling of PCM air heat exchanger," *Energy and Buildings*, vol. 38, no.2 pp. 82-89, Feb. 2006.

[29] Chan H Y, Riffat S B, Zhu J. "Review of passive solar heating and cooling technologies," *Renewable & Sustainable Energy Reviews*, vol. 14, no.2, pp. 781-789, 2010.

[30] F. Luo et al., "Optimal Dispatch of Air Conditioner Loads in Southern China Region by Direct Load Control," *IEEE Trans. Smart Grid*, vol. 7, no. 1, pp. 439-450, Jan. 2016.
[31] F. Luo, Z. Y. Dong, K. Meng, et al. "An Operational Planning Framework for Large-Scale Thermostatically Controlled Load Dispatch," *IEEE Trans. Industrial Informatics*, 2017, vol. 13, no. 1, pp. 217-227, Feb. 2017.
[32] Nagano, K., et al. "Study of a floor supply air conditioning system using granular phase change material to augment building mass thermal storage—Heat response in small scale experiments," *Energy & Buildings*, vol. 38, no. 5, pp. 436-446, May 2006.
[33] Sharma, Atul, et al. "Review on thermal energy storage with phase change materials and applications," *Renew. & Sustain. Energy Reviews*, vol. 13, no. 2, pp. 318-345, Feb. 2009.
[34] Gracia, Alvaro De, and L. F. Cabeza. "Phase change materials and thermal energy storage for buildings," *Energy & Buildings*, vol. 103, pp. 414-419, Sep. 2015.
[35] D. Z., Sun, and A. H. Oort. "Humidity-Temperature Relationships in the Tropical Troposphere," *Journal of Climate*, vol. 8, no. 8, pp.1974-1987, Aug. 1995.
[36] Weather history for Wuhan CN, Whether underground. [Online]. Available: https://www.wunderground.com/history/airport/ZHHH/

Fanrong Wei was born in Hubei, PR.China, in 1991. He received the B.Sc. degree in electrical engineering from Huazhong University of Science and Technology (HUST) in 2013. He is currently a Ph.D candidate at Huazhong University of Science and Technology (HUST). His researches mainly focus on include optimal power system/microgrid scheduling and protective relay.

Yuanzheng Li received the M.S. degree and Ph.D. degree in Electrical Engineering from Huazhong University of Science and Technology (HUST), Wuhan, China, and South China University of Technology (SCUT), Guangzhou, China, in 2011 and 2015, respectively. His current research interests include optimal power system/microgrid scheduling, stochastic optimization and multi-objective optimization.

Quan Sui was born in Anhui, PR. China, in 1995. He received the B.Sc. degree in electrical engineering from Huazhong University of Science and Technology (HUST) in 2017. He is currently a Ph.D candidate at Huazhong University of Science and Technology (HUST). His researches mainly focus on optimal power system/microgrid scheduling.

Xiangning Lin (SM'09) was born in Guangxi, PR. China, in 1970. He received the M.Sc. and Ph.D. degrees in electrical engineering from HUST. Currently, he is a Professor at HUST. His research interests are modern signal processing and power system protective relay.

Le Chen (S'17) was born in Hubei, PR. China, in 1990. He received the B.Sc. degree in electrical engineering from Huazhong University of Science and Technology (HUST) in 2013. He is currently a Ph.D. candidate at Huazhong University of Science and Technology (HUST). His research interests are power system protection and control, substation communication and cyber security.

Zhe Chen (M'95–SM'98) received the B.Eng. and M.Sc. degrees from Northeast China Institute of Electric Power Engineering, Jilin City, China, and the Ph.D. degree from University of Durham, U.K. He is a full Professor with the Department of Energy Technology, Aalborg University, Denmark. His research areas are modern power systems, power electronics and electric machines.

Zhengtian Li was born in Hubei, China, in 1979. He received the Ph.D. degree in electrical engineering in 2011 from Huazhong University of Science and Technology, Wuhan, China, where he is currently an associate Professor. His research interests mainly focus on protective relaying, power system control and analysis.